Check for updates

Post-mortem identification of lithium plating in high energy automotive batteries

Syed Muhammad Abbas, [ID] *[a] Anna Jodlbauer,[b] Martin Wilkening, [ID] [bf] Helmar Wiltsche, [ID] [c] Josef V. Ecker,[de] Christian Ellersdorfer, [ID] [a] Gregor Gstrein [ID] [a] and Ilie Hanzu [ID] *[bf]

The performance of LIBs deteriorates over time due to various aging mechanisms, among which lithium plating (LP) is critical. This study investigates LP in commercial high-energy graphite-SiO$_x$/NMC pouch LIBs cycled until end-of-life (EOL) under LP-inducing conditions. Employing post-mortem analysis techniques such as ^{7}Li nuclear magnetic resonance (NMR) spectroscopy, inductively coupled plasma optical emission spectroscopy (ICP-OES), and scanning electron microscopy (SEM), we aim to provide a comprehensive understanding of LP. Electrochemical methods such as incremental capacity analysis (ICA) and differential voltage analysis (DVA) were first used to identify LP occurrence in a cell during artificial ageing (AA). Subsequently, the cells were dissected to prepare post-mortem analysis samples. ICP-OES revealed an increased soluble lithium (Li) content on the anode surface compared to a fresh cell, which is attributed to LP. Metallic Li was identified on the anode surface of the cycled cell by ^{7}Li NMR at Knight shifts in the range from 245 to 270 ppm, whereas no metallic Li was detected in fresh cell. Post-mortem SEM analysis revealed a mossy layer growth on anode sample of the artificially aged cells that is absent on the anode surface of a fresh cell. This mossy growth is attributed to LP. Elemental mapping also revealed fluorine hotspots on the mossy metallic Li layer, indicating the formation of lithium fluoride (LiF) as a reaction product between metallic Li and the cell electrolyte. Additionally, as the SEM sample was exposed to air during transfer, oxygen hotspot on mossy Li layer in elemental mapping indicates the reaction of oxygen and moisture with metallic Li.

Introduction

First introduced by Sony corp. in 1991,[1] lithium-ion batteries (LIBs) have emerged as the leading energy storage devices due to their high energy densities, high coulombic efficiency and low self-discharge.[2,3] These properties make LIBs ideal for portable electronic devices such as cameras, laptops, and mobile phones. Additionally, LIBs are largely used in electric vehicles (EVs) and some electric grid-relevant storage applications.[3,4] However, the performance of LIBs deteriorates over their operational lifespan due to various ageing mechanisms.[5–7] This study focuses on lithium plating (LP) a critical issue affecting LIBs performance.[8,9] LP formation occurs when anode

voltage drops below 0 V *vs.* Li/Li$^+$, this situation may occur at low temperatures, high charging rates (C-rate) and localized/inhomogeneous pressure.[8–11] LP can be identified using non-destructive/*operando* methods as well as destructive/post-mortem methods.[9,12–14] A non-destructive/electrochemical identification of LP study was previously conducted in our laboratory. We were able to identify LP in high energy cells using data recorded during cycling without damaging the cell.[15] However, there were aspects that could not be clarified without opening the cell. This study employs post-mortem methods to further investigate LP. The purpose of post-mortem LP identification is to further prove the formation of LP that has been identified using electrochemical methods. Although electrochemical methods identify LP without any disturbance in the cell, the method is limited by the method used and it depends on the accuracy of recorded data for LP identification. Post-mortem analysis gives a direct detection/identification of LP as the anode is directly analyzed after cycling under LP inducing conditions, however after these investigations the cell cannot be used further.

By post-mortem analysis, LP can be identified using various techniques, including ^{7}Li nuclear magnetic resonance (NMR) spectroscopy, inductively coupled plasma optical emission

[a]*Vehicle Safety Institute, Graz University of Technology, Graz 8010, Austria. E-mail: s. m.abbas@tugraz.at*

[b]*Institute of Chemistry and Technology of Materials (NAWI Graz), Graz University of Technology, Stremayrgasse 9, Graz 8010, Austria*

[c]*Institute for Analytical and Food Chemistry, Graz University of Technology, Graz 8010, Austria*

[d]*FILL Gesellschaft m.b.H., Fillstraße 1, Gurten 4942, Austria*

[e]*EDAG Engineering Austria GmbH, Betriebspark 21, St.Ulrich bei Steyr 4400, Austria*

[f]*ALISTORE – ERI European Research Institute, CNRS FR3104, Hub de L'Energie, Rue Baudelocque, Amiens F-80039, France*

spectroscopy (ICP-OES), X-ray photoelectron spectroscopy (XPS), scanning electron microscopy (SEM), atomic force microscopy (AFM).[13,14,16–18] Comprehensive summaries of post-mortem methods used to identify LP in LIBs has been provided by Waldman *et al.*,[13,19] Paul *et al.*[14] and Janakiraman *et al.*[20] that summarized post-mortem methods used to identify LP in LIBs. XPS is limited to the surface of sample as the penetration depth is very low, AFM can be used for surface imaging but no information about the surface elements can be obtained. In this study ^{7}Li NMR, ICP-OES and SEM are used to investigate LP in commercial high energy LIBs. These methods are selected based on their qualitative (^{7}Li NMR and SEM) and quantitative (ICP-OES) analysis of LP in commercial high energy LIBs as *in situ* methods cannot be applied to commercial LIBs due to the design and structure of those LIBs.

In literature, ICP-OES has been used to investigate LIBs cycled under various conditions including simulating normal driving conditions, lithium ions (Li$^+$) amount was analyzed in comparison to a fresh cell.[17] A commercial 5 Ah pouch cell was aged under laboratory conditions ranging from 25 °C to 45 °C[21,22] and a 1.95 Ah cylindrical cell at elevated temperatures of 60 °C[21] to analyze electrode composition and Li$^+$ content was analyzed to investigate capacity loss. It is important to remember that ICP-OES detects all soluble Li$^+$ that can be contributed by SEI, residual electrolyte and LP. Ecker *et al.*[23] conducted a post-mortem analysis on a commercial 40 Ah pouch graphite/NMC cell cycled at −10 °C with constant current-constant voltage (CC-CV) protocol until the cell reached state of health (SOH) 80% based on residual capacity. Their study use ICP-OES and laser microscopy for post-mortem analysis to determine the effect of operation condition on LP. ^{7}Li NMR has been used for *in situ* quantification of dead lithium (Li) and Li corrosion, formation of metallic Li and *operando* Li deposition in laboratory fabricated NMC811/graphite cell.[24–27] SEM microscopy has been used to observe the morphology of deposited Li on anode samples of experimental cells.[28–33] A 1.5 Ah 18650 NMC-LMO/graphite cell cycled at 25 °C and anode was studied under SEM to investigate temperature dependent ageing.[34] SEM was used for surface morphology of 1.95 Ah 18650 NMC/graphite cell cycled at 20 °C to study LP and non LP anode areas.[22] Low temperature effect on anode surface were also analyzed using SEM in a 15 Ah pouch cell.[35] Zhang *et al.*[18] conducted post-mortem analysis of a prismatic cell at −10 °C using SEM and XPS to identify and observe LP growth morphology.

Unfortunately, a comprehensive post-mortem investigation of commercial high energy graphite-SiO$_x$/NMC pouch LIBs cycled under LP boundary conditions (BCs) has not been reported in the literature. The objective of this study is to perform post-mortem investigation of LP in commercial graphite-SiO$_x$/NMC pouch LIBs using ^{7}Li NMR, ICP-OES and SEM. ICP-OES give a quantitative analysis of the total Li on the surface of anode originating from LP, SEI and residual electrolyte. Please note that the speciation of Li on the surface may also be different. While LP leads to metallic Li, the Li from the SEI and the residual electrolyte is in ionic form. Nevertheless, ^{7}Li NMR is able to distinguish between ionic and metallic Li resulting in

direct identification of LP. SEM reveals the morphology and growth of LP on surface of graphite particles while by EDXS fluorine and oxygen elemental mapping indirectly reveal LP spots. In this study, the pouch cells were artificially aged (AA) until their end of life (EOL) state-of-health (SOH) under LP boundary conditions (BCs). In addition, this research validates the findings in our previous study[15] where only non-destructive electrochemical methods were used to identify LP.

Methodology

Cell cycling conditions leading to LP were already established in our previous research.[15] A set of LP inducing BCs were selected based on the feasibility to be applied in our laboratory for extended number of cycles, the cells were cycled at 15 C and 10 °C temperature, between state of charge (SOC) 0% and 90% till SOH less than 85% was achieved. There, in ref. 15 we used electrochemical methods such as incremental capacity analysis (ICA) and differential voltage analysis (DVA) to identify LP. The same selected electrochemical methods are applied to cell cycling data in order to investigate the occurrence of LP, building upon the analysis discussed in our previous study.[15]

In addition, the approach for post-mortem identification of LP was based on quantitative and qualitative methods. ICP-OES distinguishes between elements based on their optical emission and quantifies the amount of constituent elements. In this research, LP was detected from water soluble Li$^+$ and fluorine ions (F$^-$) are recorded in ICP-OES and ion chromatography respectively. Indeed, any metallic Li can be also eluted when a known electrode surface is washed with a known quantity of distilled water. A higher amount of Li$^+$ found from AA anodes, in comparison to fresh cell, indicates LP. This argument is also supported by F$^-$ content on the anode, as electrolyte decomposition products on metallic Li, especially lithium fluoride (LiF),[36] leads to an decreased F$^-$ content in the eluted mass. Indeed, LiF is an insoluble compound. ^{7}Li NMR can directly identify LP by distinguishing Li in diamagnetic environments from metallic Li. In metallic Li, the conduction electrons create a local magnetic field at the nuclear sites due to their spin polarization. This hyperfine interaction between the nuclear spins and the conduction electrons leads to a diagnostic Knight shift in the NMR resonance frequency. Unlike the (isotropic) chemical shift, which depends on the local magnetic environment in (diamagnetic) ionic compounds, the Knight shift in metals is caused by the Fermi contact interaction. This interaction results in a significant upfield shift (higher resonance frequency) for metallic Li compared to so-called ionic lithium, which is, *e.g.*, found in the electrolyte and the SEI.[36]

SEM and elemental mapping are used to indirectly identify LP after the samples have been exposed to air. SEM reveals surface morphology of the AA anode and it can be compared to the surface morphology of a fresh and real aged (RA) anode. SEM backscattered electrons images are presented in this study. Although SEM-EDX cannot identify Li, elemental mapping of oxygen (O) and fluorine can help indirectly indicate LP because electrolyte and LP reaction leads to oxygen and fluorine containing by products.[36,37] These by products are concentrated on

Table 1 Cell specifications and boundary conditions

Cell model	Lithium-ion battery – pouch
Cell structure (stacked layers)	66 separators (alumina coated), 33 anodes and 32 cathodes
Chemistry	NMC712/graphite + SiO_x
Capacity	64.6 Ah
Nominal voltage	3.65 V
Maximum voltage	4.25 V
Minimum voltage	2.8 V
Boundary conditions	
Test protocol	CC-CV
C-rate	1.5 C
Temperature	10 °C
SOC limit	0-90-0%

LP areas on anode surface and appears as a hotspot of relative high concentration of oxygen and fluorine elements in elemental mapping.

ICP-OES provide quantitative analysis of the Li^+ and F^- species in the anode, a difference in the amount indirectly indicating the formation of metallic Li. ^{7}Li NMR directly identifies LP, by the very distinct Knight shift of metallic Li. Please note that, on the one hand, both ICP-OES and ^{7}Li NMR provide information on LP averaged over the chosen sampling area, which is relatively large. On the other hand, SEM-EDX scan area range from mm to nm scale, providing a very localized analysis of LP on the surface of anode. Our selected methods have the advantage of providing elemental composition, direct LP identification, on both a localized area and a larger area, where fluctuations are averaged. Of course, there are some other experimental techniques that could be used, such as AFM and XPS. While these techniques are highly surface sensitive, they also have some disadvantages. For instance, AFM does not provide elemental composition at all. In the case of XPS, only the surface chemical composition, *i.e.* on nm scale, is determined. Thus, in both case the information is very localized in comparison to NMR. In addition, the preparation of samples for AFM and XPS is much more complex than for our chosen methods and, XPS in particular, requires handling of samples under a highly pure inert atmosphere. Other *in situ* methods require the analysis during cycling of the cell which was not possible with commercial large format cells. Thus, although there are for sure methods that are able to provide much more localized and accurate information, we believe that our choice of methods is the most judicious in terms of sample preparation, easiness of interpretation as well as an overall reduced complexity and improved reproducibility. Such a choice is most likely best suited for the analysis of commercial cells, offering a good balance in terms of experiment complexity – data quality ratio.

Experimental

This study was conducted using the same commercial high energy pouch LIBs as in our previous study.[15] The specifications are described in the Table 1. The cells were cycled while kept under external mechanical pre-tension and a localized pressure area to induce localized LP,[10,30,38] two cells were cycled at the same time with a parallel connection and the setup is described in Fig. S1. The localized high-pressure area was introduced in the cells in order to evaluate the effects of inhomogeneous pressure on LP. Thus, localized inhomogeneous pressure is an additional boundary condition to trigger localized LP. SEM and ^{7}Li NMR samples taken from the localized pressure area were compared with samples taken from normal pressure areas. The cells were subjected to a CC-CV charge–discharge protocol with a cut-off current limit in the CV phase set at C/10. Prior to the cycling, the cells were discharged to SOC 0% and rested for 15 minutes. An electrochemical characterization (EC) cycle using CC-CV protocol at 0.5C was then conducted as described in Fig. S2. Following this EC, test cycling commenced. In the 1st cycle, the cells were charged to SOC 90% followed by a relaxation time of 1.5 hours and subsequently discharge cycle to SOC 0%. In the next 4 cycles, the cells were charged to SOC 90% and discharged to SOC 0% without any relaxation time following the charge cycle. This protocol was repeated every 5 cycles. The cycling continued until cell reached a SOH between 80% and 85%. The detailed cycling procedure is described in Fig. S2(a–c). The BCs are derived from previous study[15] are shown in Table 1. To distinguish the cells used in this study based on their different ageing history, a nomenclature is provided in Table 2.

LP has been identified in the cycled cells using electrochemical non-destructive methods as described in our previous study.[15] Characteristic LP peak has been identified in ICA and DVA curves, see Fig. S3.

Post-mortem analysis anode samples were prepared under inert environment. As LP only occurs on the negative electrode (the anode), the separator and cathode were not used for post-mortem analysis. The cycled cell was dissected in an argon filled glove box, with O_2 and H_2O levels ≤0.5 ppm, to prevent exposure of cell components to air and moisture. Samples for ^{7}Li NMR qualitative analysis were only taken form anode layer 1 and 7, counting from the cell exterior on the impactor side, see

Table 2 Cell nomenclature and ageing history

Cell nomenclature	SOH	History
Fresh (F)	100%	Fresh cell, not used in application
Real aged (RA)	93%	Used in a car for *ca.* 160000 km
Artificially aged not stored (AA_NS)	85%	20 cycles under LP conditions, cell dissected immediately after cycling
Artificially aged stored (AA_S)	82%	20 cycles under LP conditions, cell stored for 11 weeks and then dissected

Fig. S4(a). As ICP-OES and ion chromatography are quantitative methods, anode layer 2, 4, 8, 16 and 32 were sampled to investigate Li$^+$ content in different layers of the cell, see Fig. S4. Another reason to use multiple sample layers for ICP-OES/ion chromatography was to investigate the effect of temperature on LP formation as the temperature increase when we approach layer 32, see Fig. S4. SEM and elemental mapping sample was prepared from anode layer 5. For ^{7}Li NMR and ICP-OES, samples were collected from the middle and tab side of each layer to investigate the effect of localized pressure as the tabs side of the cell is at lower pre-tension as compared to the middle, see Fig. S5. SEM sample sized 1 cm × 1 cm was prepared from middle of the anode to include the localized pressure area, the nominal pressure area and the boundary between the two regions, see Fig. S5.

For ^{7}Li NMR samples preparation, the anode active material was mechanically detached from the copper current collector by scrapping it off with a scalpel, taken to 2.5 mm zirconia NMR rotor tubes that were filled and sealed in the glovebox. ICP-OES samples were prepared by cutting the anode samples, weighing them and subsequently immersing them in 50 mL of water outside the glove box to disperse the active material particles and dissolve the soluble compounds, including the metallic Li that reacted with water. The resulting current collector that was completely stripped of its active material film, was weighed again to determine the mass of the active material film (calculated as the difference in weight before and after removal of the active film layer). The active material dispersed into water was separated by centrifugation and the clear solutions were used further for ICP-OES measurements. The anode sample for FESEM-EDXS was sealed in a pouch for transport and prepared for analysis under ambient conditions. The potential reaction of the active material with air was accounted for during the SEM-EDX analysis.

High-resolution NMR measurements were performed under magic angle spinning (MAS) conditions using a Bruker Avance spectrometer connected to a shimmed cryomagnet with a nominal field of 11.7 T. For acquiring ^{7}Li (spin-quantum number $I = 3/2$, 194.4 MHz) MAS NMR spectra, a spinning speed of 25 kHz was chosen, with a delay time of 0.3 seconds and a total of 2048 scans per sample. The resulting free induction decays were transformed into the frequency domain via Fourier transformation without further modifications. Polycrystalline lithium acetate (CH$_3$COOLi) was used as the reference material to determine the isotropic chemical shifts in the ^{7}Li NMR spectra.

Li was quantified by ICP-OES (Arcos II, Spectro, Germany) in radial plasma viewing. The Li I 670 780 nm emission line was used. For instrument calibration, 5 external calibration solutions in the range of 0.1 to 10 mg L^{-1} were used. They were prepared from a 1 g L^{-1} Li-stock solution (Merck, Germany) and diluted (3 mol L^{-1}) nitric acid. The samples were diluted with 3 mol L^{-1} nitric acid (high purity nitric acid produced by sub-boiling reagent-grade HNO$_3$ in a quartz still) prior to analysis. Fluoride content was determined by ion chromatography. The samples were diluted with carrier solution (4 mmol L^{-1} Na$_2$CO$_3$ + 1 mmol L^{-1} NaHCO$_3$) prior analysis. A Shodex IC SI-50 4E

Anion-Column and a SeQuant CARS (Merck Millipore, Sweden) suppressor were combined with a conductivity detector (Shimadzu, Japan). 5 external calibration standards in the range 0.5–20 mg L^{-1} were prepared from a 1 g L^{-1} fluoride stock solution (Merck, Germany) by dilution with carrier solution. Samples were filtered with Chromafil Xtra IC-45/25 (Machery-Nagel, Germany) syringe filters prior dilution to prevent the introduction of graphite particles onto the separation column.

Surface morphological analysis of the anode samples was performed using scanning electron microscope (SEM). Alongside surface morphology analysis, elemental mapping of the sample surface was also conducted at various magnifications. Both SEM and elemental mapping were carried out using a Zeiss Ultra 55 field emission scanning electron microscope (FESEM) equipped with an EDAX Super Octane system for energy-dispersive X-ray spectroscopy and elemental mapping.

Results

The ICP-OES and ion chromatography analysis results show the water-soluble Li$^+$ and F$^-$ content in fresh, real aged (RA) and accelerated aged (AA) cells, Fig. 1(a and b). These analysis shows water soluble Li and F content on the anode sample[17] The soluble Li$^+$ and F$^-$ species have their origin from three internal sources, namely LP, SEI and residual electrolyte on the anode sample.[23,36,39] In Fig. 1(a), it can be observed that fresh cell shows the lowest soluble Li$^+$ content, whereas real aged cell shows Li content similar to AA_NS cell and lower than AA_S cell. For AA cells, stored cell shows higher Li$^+$ content as compared to not stored cell. The soluble Li$^+$ content in an AA cell is constant or slightly decreasing as we move from layer 2 to 32 (we move form cold side of the cell, kept at 10 °C to the warm that may reach 22 °C, see Fig. S4). It is also important to note that sample taken from middle or side of the same anode layer shows no significant difference in Li$^+$ content. This was unexpected, since the pressure in the middle of the cell was intentionally set to higher values by the use of a well-defined impactor. It seems that in the used pressure range, the soluble Li content is not influenced by the pressure. In Fig. 1(b), it is observed that the soluble F$^-$ content is lower in fresh cell as compared to RA and AA cells. The F$^-$ content is similar for real aged and AA, as F$^-$ content is primarily sourced from SEI and residual electrolyte. AA_S shows higher F$^-$ content as compared to AA_NS cell. The F$^-$ content also slightly decreases from anode layer 2 to 32 and no significant difference is observed between sample from middle or side of the anode layer. Two main reaction products of LP and electrolyte are LiF and Li inorganic carbonates[36] which are both non-soluble in water. Thus, formation of LiF compound reduces both Li$^+$ and F$^-$ content in ICP-OES and ion chromatography analysis, the soluble species from the liquid electrolyte are consumed.

Please note that no replicate experiments were conducted for Li plating. However, we know from our previous study,[15] that Li plating response is highly reproducible under the chosen conditions. Since a relatively large area, typically in the order of 100 × 100 mm^2 was sampled for elemental analysis, the values that are presented in Fig. 1 are average values over the samples
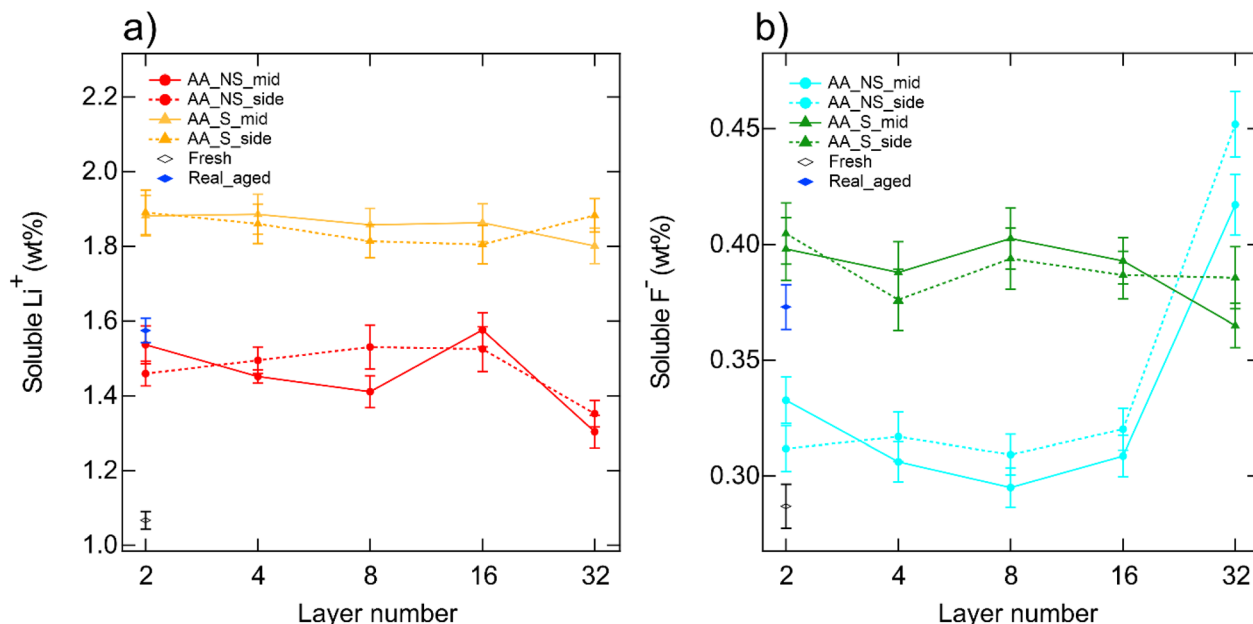
Fig. 1 ICP-OES and ion chromatography analysis of anode samples from fresh, real life aged (RA) and artificially aged (AA) cells, with error bars. (a) The water-soluble Li^+ content in the anode active material film and (b) the water-soluble F^- content in the anode material film. The values are expressed as weight % relative to the mass of the active material film. The mass of the active material film also includes the remaining electrolyte as the active films were processed without further treatment after cell opening.

surface. The ICP-OES and ion chromatography determination error was 1–3% for Li^+, and approximately 3.5% for F^-.

In Fig. 2(a and b), ^7Li MAS NMR spectra of the active materials of the distinct cells are compared. Li NMR lines mirroring

Li^+ in non-metallic environments can be observed for fresh, real aged and AA cells at chemical shifts close to 0 ppm,[25,30,40] see Fig. 2(a). In contrast to ionic Li, the characteristic ^7Li NMR line representing metallic Li is observed at Knight shifts ranging
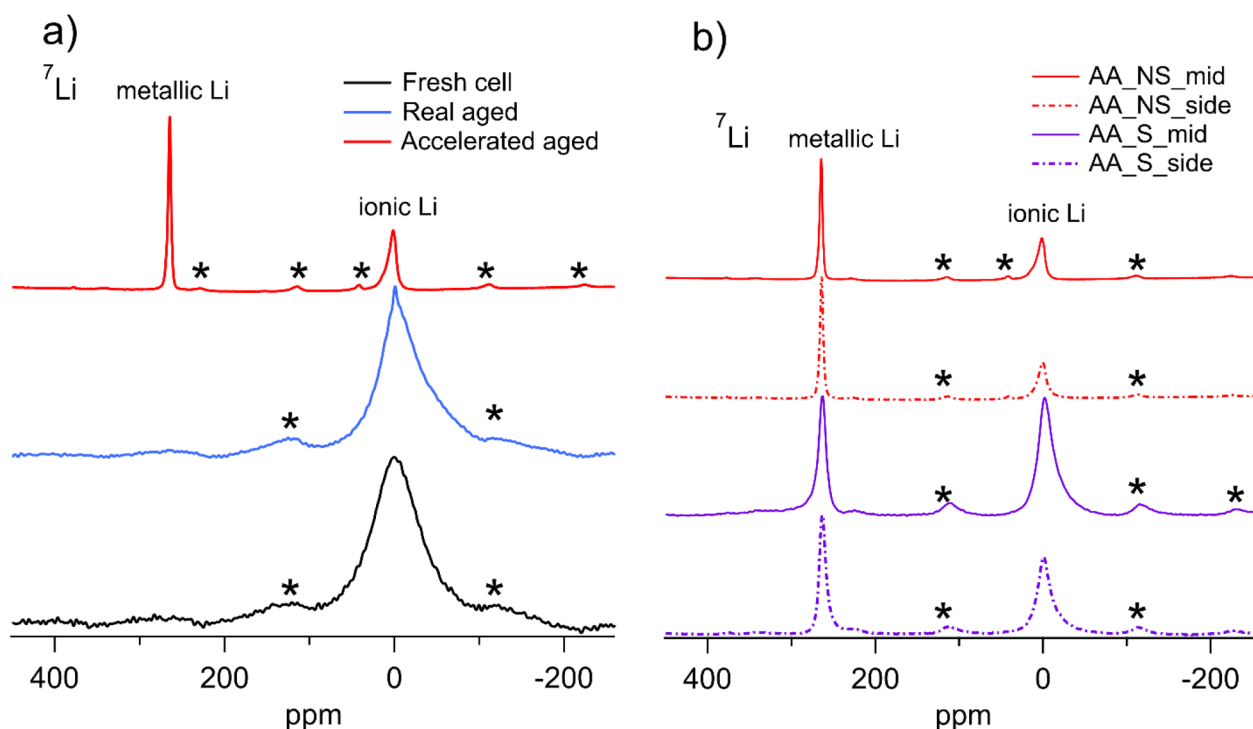
Fig. 2 ^7Li MAS NMR spectra. (a) Comparison of fresh, real life aged (RA) and accelerated aged (AA) cell, (b) AA cells with different storage history and sample position. The "S" letter indicates cells that after accelerated ageing were stored for 11 weeks while "NS" indicates non-stored cells, *i.e.* cells that were opened the same day after the accelerated ageing was completed. The lines marked with asterisks reflect spinning side bands.
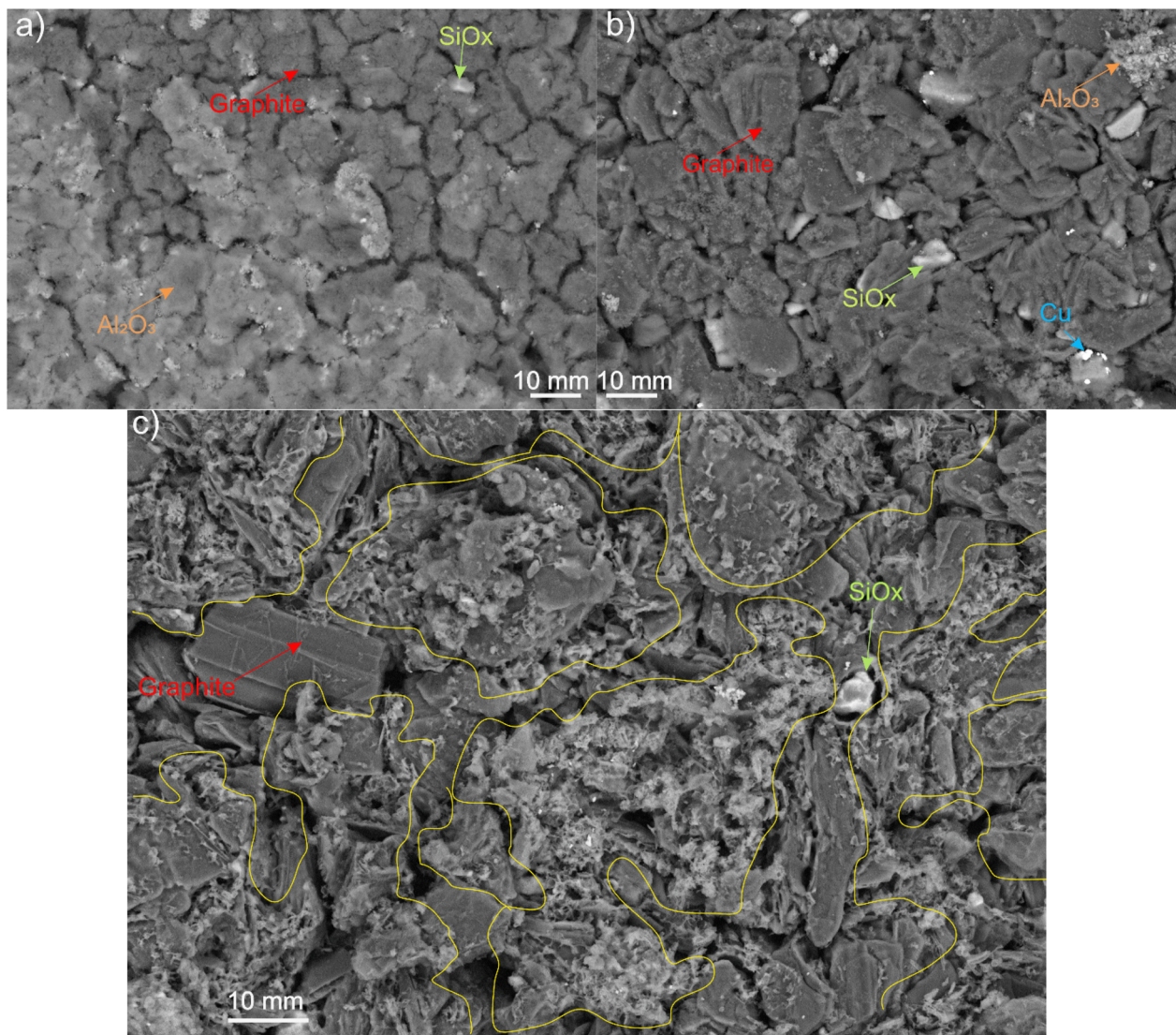
Fig. 3 SEM anode surface morphology comparison of different cells. (a) Fresh, (b) real aged and (c) AA. A mossy layer, on top of the accelerated aged sample can be distinguished. This layer, absent in fresh and real aged cells, is the result of lithium plating and can be identified as the remains of mossy Li plating after air exposure during sample transfer to the SEM.

from 245 to 270 ppm.[24–26,41] In the AA anode sample, however this characteristic peak is not observed in anode samples from fresh and real aged cells. As mentioned above, for metallic Li the Knight shift is very large and, thus, clearly distinct from the chemical shifts of ionic Li species. This finding unequivocally confirms LP during cycling under the applied BCs in AA cells. The side bands observed in the spectra, marked with a '*', are the result of higher order terms present in the dipolar, chemical shift anisotropy and quadrupolar interactions at a rotation speed of approximately 25 kHz. The first order terms are significantly averaged-out by the fast rotation of the sample, leading to much narrower main resonance lines, as shown in Fig. 2.

In Fig. 2(b), anode samples from both stored and non-stored AA cells exhibit a characteristic NMR line revealing metallic Li. Metallic Li is identified in samples taken from middle of the anode layer as well as samples from tab side of the layer (towards the tab) of the same layer. In all collected samples from AA cells, a strong metallic Li NMR line is observed at 245–270 ppm.

SEM surface morphology comparison between fresh, real aged and AA anode samples is shown in Fig. 3(a–c). Graphite particles are identified in darker shade, whereas SiO_x particles are observed in lighter shade (using the back scattered electron detector), this is due to higher atomic mass of silicon (Si), see Fig. 3(a–c). Copper (Cu) residue is also observed on graphite particles in real aged sample, possible a result of current collector corrosion, see Fig. 3(b). Also, some Al_2O_3 residues, very likely from the separator coating are found on both fresh and real aged sample, Fig. 3(a and b). Most importantly, in Fig. 3(c), a mossy layer (marked with a yellow boundary) found on top of graphite particles[29,33] can be distinguished only on AA sample,
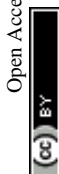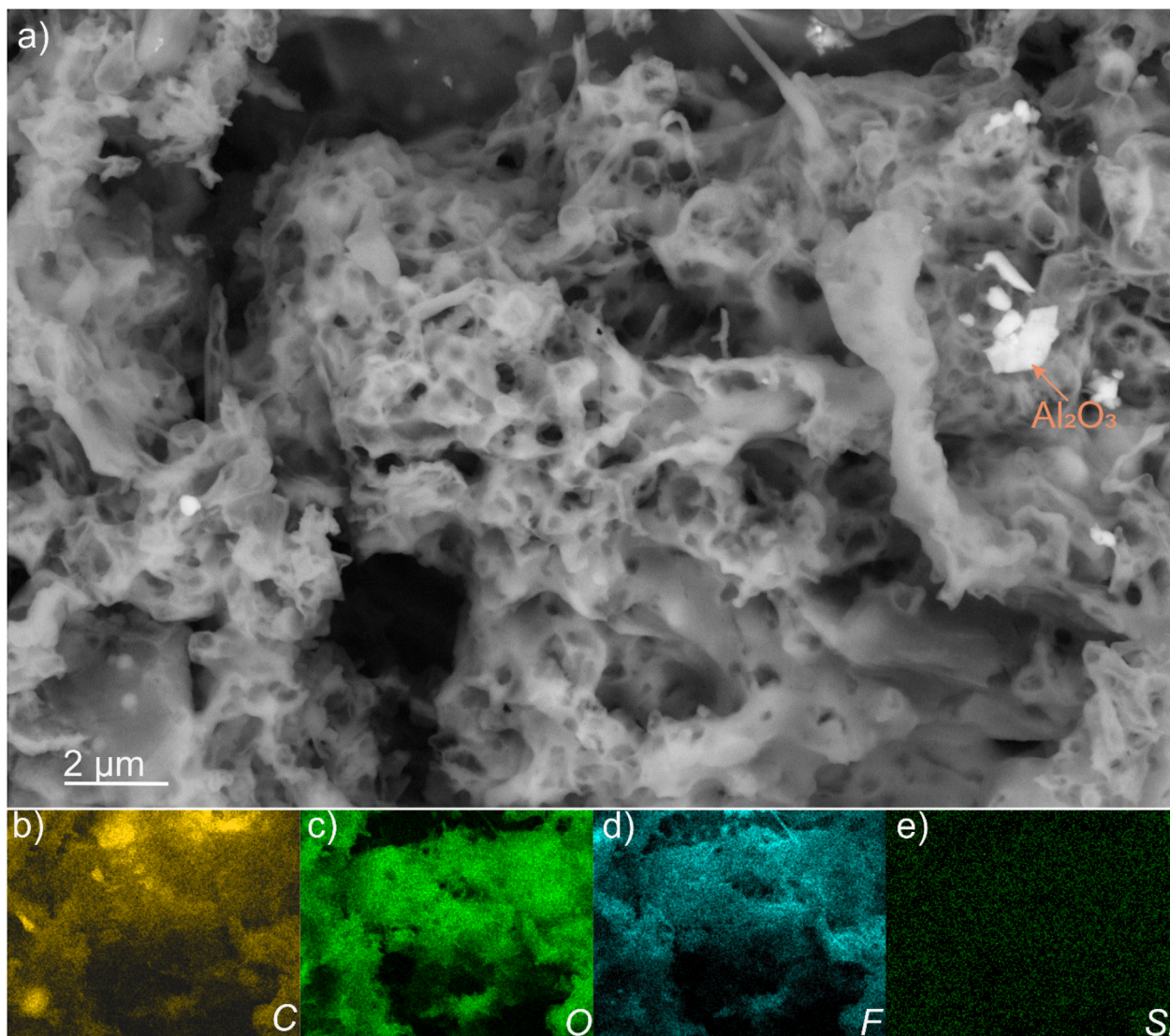
Fig. 4   SEM higher magnification surface morphology and elemental EDX mapping of AA anode sample. (a) surface morphology, (b–e) elemental mapping of carbon, oxygen, fluorine and silicon respectively.

while on fresh and real aged samples it is absent, see Fig. 3(a and b).

Higher magnification SEM images are shown in Fig. 4(a) along with elemental mapping, Fig. 4(b–e). The higher magnification Fig. 4(a) provides a clear insight into the remains of the metallic Li layer that grew on graphite particles. Elemental mapping of fluorine and oxygen correlates very with each other, Fig. 4(c and d). Oxygen hotspots overlap fluorine hotspot, whereas a weaker carbon signal is recorded from the same sample area due to LP covering the graphite particle, in comparison to the bright areas where graphite surface is visible, see Fig. 4(b).

Discussion

In Fig. 1(a and b) the ICP-OES and ion chromatography analysis shows the variation of soluble Li^+ and F^- content respectively, across different anode layers of the AA cell, compared with fresh and real aged cells. The Li^+ detected is attributed to the plated Li that reacts with water and dissolves completely, the water-soluble Li-containing SEI (solid electrolyte interphase) products and residual electrolyte.[23,36] The real aged cell also shows higher soluble Li^+ content, this can be attributed to thicker SEI as compared to fresh cell, as ^7Li NMR and SEM confirms no LP occurs in real aged cell. In Fig. 1(a), the trend indicates that soluble Li^+ content in AA cell is stable or slightly decreases from layer 2 to layer 16 and decreases in layer 32. This decrease can be attributed to 10 °C temperature positive gradient during cycling as we move from layer 2, kept at 10 °C, to the warmer layer 32, where the temperature may exceed 20 °C (due to the cell self-heating during charging), see Fig. S4. As higher temperatures result in reduced LP, thus a lower Li^+ content on the anode is expected on layers where the temperature is higher. Comparing non-stored (AA_NS) and stored (AA_S) cells, it can be observed

that AA_S presents a higher soluble Li$^+$ content, which can be attributed to comparatively lower SOH of AA_S after cycling under LP boundary conditions, see Table 2. A lower SOH after cycling is a result of higher amount of LP under the applied BCs. As confirmed by NMR (see below) it can be concluded that even after storage of 11 weeks, AA_S cells have metallic Li on anode surface. This result is surprising since it would be expected that finely divided plated Li would either partially resorb into graphite or, after a while, would react with the electrolyte and convert into SEI. Yet, the few weeks of storage is clearly not sufficient to remove all metallic Li from a cell cycled under LP conditions. This finding points towards long-lasting consequences following a LP event. Indeed, a cell that contains metallic Li is expected to have a narrower operational safety envelope.

In Fig. 1(b), F$^-$ content is shown to decrease until layer 8 as metallic LP reacts with electrolyte forming the insoluble LiF compound, resulting in a lower soluble F$^-$ content. In AA_NS, as we move to layer 16 and 32 the cell temperature increases, leading to a relatively lower LP. Since the metallic Li quantity is lower on layer 32 than on layer 16, it results in a lower amount of electrolyte decomposition by reacting with metallic Li, hence increase in F$^-$ content that can be traced to the higher electrolyte content on layer 32. This cell is dissected immediately without storage after cycling for sample preparation, therefore a higher concentration of F$^-$ is left on anode number 32 surface. For the AA_S cell, during storage, LP gradually reacts with electrolyte forming LiF, hence the slightly decreasing trend of F$^-$ content across all layers.

^{7}Li NMR analysis shows no presence of metallic Li in fresh and real aged cells, Fig. 2(a). Metallic Li is observed only in AA cell anode samples, indicating that the test BCs were suitable for LP formation as compared to real ageing conditions. Metallic Li is found around 245–270 ppm as compared to ionic Li at 0 ppm.[2,24–26] In Fig. 2(b), metallic Li is observed in both types of AA cell, demonstrating that storage after cycling does not remove metallic Li in the cells that were cycled within LP boundary conditions, with significant metallic Li remaining after relatively long storage. Within the same layer, there is no significant difference, as LP is observed in both the middle of the layer and on the tab side. ^{7}Li NMR provides direct confirmation of the presence of metallic Li in the cells cycled under applied BCs. The slight difference in metallic Li peak position in Fig. 2(b) can be attribute to orientation of metallic Li.[25] In addition, this finding further confirms the previous non-destructive identification of LP using electrical measurements only, that constituted the subject of a previous study.[15]

SEM analysis reveals differences in the surface morphology between fresh, real aged and AA anode samples, see Fig. 3(a–c). This mossy layer can be attributed to LP on the anode surface, and it is clearly distinguishable from fresh and real aged sample.[29,30,35,42,43] This mossy growth is identified as LP, outlined in Fig. 3(c). As the SEM sample was prepared in ambient atmosphere, it is expected that the metallic Li has reacted with air and moisture forming Li-carbonates and Li-hydroxide[37] products on the mossy metallic Li. LP also is covered by reaction decomposition products of LP and electrolyte containing

fluorine. Thus, LP can be indirectly identified using oxygen and fluorine elemental mapping. In addition, Fig. 3(a and b) shows clearly identified SiO$_x$ particles in anode active material, along with Al$_2$O$_3$ residue from separator during sample preparation.

In higher magnification images in Fig. 4(a), the morphology of LP is analyzed, revealing a mossy growth rather than dendritic growth,[30] this growth behavior is likely a consequence of low test temperatures and C-rate.[42] The elemental mapping signal from carbon is weaker due to LP on graphite particle that obscures the graphite underneath, see Fig. 4(b). Exposure of the SEM sample to air during preparation oxidized metallic Li, forming Li-carbonate and Li-hydroxide layers which consequently result in an oxygen hotspot on the area where LP has occurred, Fig. 4(c). Oxygen almost absent on unobscured graphite, while the oxygen signal is strong on mossy Li areas, which are perfectly overlapping with areas where fluorine content is higher. Indeed, as metallic Li surface covers also with LiF after reacting with electrolyte, elemental mapping shows higher fluorine content in the mossy Li area. In conclusion, the overlapped fluorine and oxygen hotspots are the clear signature of metallic Li that was electroplated on the anode, see Fig. 4(c) and (d). As a final note, the topography of the Li deposit and its relative orientation with respect to the EDX detector also affect the elemental mapping signal strength. For instance, as a weak signal can be observed from the middle bottom in Fig. 4(b–d), due to a depressed region in this area, resulting is a weaker X-ray signal reaching the detector.

ICA and DVA electrochemically confirm the formation of LP during cycling under LP condition as characteristic Li peaks, as shown in Fig. S3 and discuss in detail in a previous study,[15] the LP is further confirmed through ^{7}Li NMR, ICP-OES and ion chromatography analyses. Additionally, SEM and elemental mapping corroborate the formation of LP. The post-mortem methods are complementary to each other as ICP-OES indirectly identifies LP with Li content, ^{7}Li NMR provides direct proof of metallic Li on anode surface. SEM and elemental mapping reveal the morphology of LP and indirectly identify LP respectively.

In general, LP may occur at the anode at high cell voltages once the LP inducing BCs are achieved. While in this study, we have investigated one particular cell chemistry and one cell design, LP events are for sure possible in other cell chemistries and designs. As the cell operation voltage window of a cell is dictated the cell chemistry, it is certain that the cell voltage where LP occurs will depend on the cell chemistry. For C-SiO$_x$/NMC or C/NMC chemistry it occurs after 4 V, as demonstrated in previous studies.[15,44] Then, it is expected that the boundary conditions for LP will depend on the cell design. For instance, we can easily imagine that, in a cell designed for high power operation, LP will occur at much higher C-rates at the same temperatures, in comparison with cells designed for high energy applications. Usually, cylindrical cells are normally rated for high C-rate applications while prismatic cell for moderate C-rate application. Since temperature is also a key boundary condition for LP, one can expect to see significant differences between cylindrical, prismatic and pouch cell battery technology implementation. Indeed, as the thermal conductivity

and thermal flux may depend on the geometry of the cell, it is expected that not only the temperature BC will change from one geometry to another, but also the LP internal distribution within the cell may be different, especially if a known temperature gradient is present. Thus, we can conclude that for each cell type a different set of BCs will be required for the investigation of LP.

Conclusion

This study investigated lithium plating (LP) in high-energy commercial lithium-ion batteries (LIBs) through cycling until end-of-life (EOL) state-of-health (SOH) under LP boundary conditions (BCs). LP was first identified by incremental capacity analysis (ICA) and differential voltage analysis (DVA) as non-destructive methods. Afterwards the cell was dissected and post-mortem cell analysis was performed. Inductively coupled plasma optical emission spectrometry (ICP-OES), ion chromatography, ^{7}Li nuclear magnetic resonance (NMR) and scanning electron microscopy-energy dispersive X-ray spectroscopy (SEM-EDXS), were employed to elucidate the mechanisms and extent of LP.

Post-mortem analysis confirmed LP under the applied boundary conditions. ICP-OES revealed a higher water-soluble lithium ion (Li^+) content in artificially aged (AA) cells as compared to fresh and real aged cells. The difference in SOH between AA_NS (non-stored) and AA_S (stored) cell is evident, with AA_S exhibiting lower SOH due to higher LP, hence higher amount of Li^+ content that can be eluted with water from the electrode. The presence of metallic Li was directly confirmed by ^{7}Li NMR in AA cells. SEM revealed the morphology of the LP on graphite particles, identifying the mossy layer type of LP. Elemental mapping of fluorine and oxygen provided indirect confirmation of metallic lithium, highlighting the areas affected by LP.

Our study reveals that LP can be identified in post-mortem analysis in commercial high energy LIBs even at SOC 0% (fully discharged state). Interestingly, once lithium (Li) has been plated in the cell, we show for the first time that it remains in metallic Li form for at least 11 weeks. ICP-OES and ion chromatography can indirectly identify LP based on soluble Li^+ and F^- content in the anode when anode active material layers are dispersed in water. It was possible through ^{7}Li NMR to directly and unequivocally identify the presence of metallic Li in the anode active material of an accelerated aged cell, while no metallic Li was found in a fresh cell anode. SEM revealed the morphology of LP formations under the selected boundary conditions. It was possible to indirectly identify LP by corroborating oxygen and fluorine EDX elemental mapping. The selected methods also had inherent limitations, ICP-OES and ion chromatography as quantitative methods detect only water-soluble Li^+ and F^- content for indirect LP identification. ^{7}Li NMR provides direct LP identification but is limited as a qualitative method only. Although SEM reveals the morphology of LP, it is unable to perform direct Li elemental mapping, although elemental mapping of other elements (oxygen and fluorine) is indirectly pointing towards LP.

The unequivocal identification of LP in our study can serve as a basis for an enhanced battery management system (BMS) that can eventually become aware of LP occurrences. In principle, the BMS can detect the LP by comparing the on-line cycling data with a set of BCs that were previously determined by the method that we presented in this manuscript. The BMS can also consider the ageing of the cell that will lead to different BCs. Furthermore, in a more advanced design, based on LP data as in this study, the BMS can define absolute limits, so called "no go" conditions for battery operation. These can be segmented at the battery pack, module and individual cell level. For instance, once LP was detected in a single cell, an advanced BMS can either declare it faulty, reduce its operation envelope to safer levels, and report it for service. Thus, our study may constitute a foundation for a general LP protection and handling by the BMS.

Author contributions

Syed Muhammad Abbas contributed to the conceptualization, methodology, investigation, data analysis, writing – original draft and editing. Anna Jodlbauer contributed to NMR investigation and writing – review. Martin Wilkening contributed to NMR investigation and writing – review. Helmar Wiltsche contributed to ICP-OES and ion chromatography investigation – writing – review. Josef V. Ecker contributed to writing – review. Christian Ellersdorfer contributed to project administration, funding acquisition and writing – review. Gregor Gstrein contributed to supervision, conceptualization, methodology and writing – review. Ilie Hanzu contributed to supervision, conceptualization, methodology, data analysis and writing – review.

Conflicts of interest

The authors declare no competing financial interest.

Abbreviations

LIB	Lithium ion battery
LP	Lithium plating
VRP	Voltage relaxation profile
DVA	Differential voltage analysis
ICA	Incremental capacity analysis
CC	Constant current
CV	Constant voltage
C-rate/C	Charging rate
BCs	Boundary conditions
^{7}Li NMR	Lithium-7 nuclear magnetic resonance spectroscopy
ICP-OES	Inductively coupled plasma optical emission spectroscopy
FESEM-EDXS	Field emission scanning electron microscopy-energy dispersive X-ray spectroscopy

Data availability

Data will be made available on reasonable request.

Supporting information: Additional experimental details, results and schematics of experimental methods. See DOI: https://doi.org/10.1039/d5se00509d.

Acknowledgements

References

1 B. A. Johnson and R. E. White, Characterization of commercially available lithium-ion batteries, *J. Power Sources*, 1998, **70**, 48–54, DOI: 10.1016/S0378-7753(97)02659-1.

2 J. B. Goodenough and Y. Kim, Challenges for Rechargeable Li Batteries, *Chem. Mater.*, 2010, **22**, 587–603, DOI: 10.1021/cm901452z.

3 J. M. Tarascon and M. Armand, Issues and challenges facing rechargeable lithium batteries, *Nature*, 2001, **414**, 359–367, DOI: 10.1038/35104644.

4 B. Scrosati, J. Hassoun and Y.-K. Sun, Lithium-ion batteries. A look into the future, *Energy Environ. Sci.*, 2011, **4**, 3287, DOI: 10.1039/C1EE01388B.

5 C. R. Birkl, M. R. Roberts, E. McTurk, P. G. Bruce and D. A. Howey, Degradation diagnostics for lithium ion cells, *J. Power Sources*, 2017, **341**, 373–386, DOI: 10.1016/j.jpowsour.2016.12.011.

6 R. Xiong, Y. Pan, W. Shen, H. Li and F. Sun, Lithium-ion battery aging mechanisms and diagnosis method for automotive applications: Recent advances and perspectives, *Renewable Sustainable Energy Rev.*, 2020, **131**, 110048, DOI: 10.1016/j.rser.2020.110048.

7 J. Vetter, P. Novák, M. R. Wagner, C. Veit, K.-C. Möller, J. O. Besenhard, M. Winter, M. Wohlfahrt-Mehrens, C. Vogler and A. Hammouche, Ageing mechanisms in lithium-ion batteries, *J. Power Sources*, 2005, **147**, 269–281, DOI: 10.1016/j.jpowsour.2005.01.006.

8 N. Legrand, B. Knosp, P. Desprez, F. Lapicque and S. Raël, Physical characterization of the charging process of a Li-ion battery and prediction of Li plating by electrochemical modelling, *J. Power Sources*, 2014, **245**, 208–216, DOI: 10.1016/j.jpowsour.2013.06.130.

9 Y. Tian, C. Lin, H. Li, J. Du and R. Xiong, Detecting undesired lithium plating on anodes for lithium-ion batteries – A review on the in-situ methods, *Appl. Energy*, 2021, **300**, 117386, DOI: 10.1016/j.apenergy.2021.117386.

10 G. Fuchs, L. Willenberg, F. Ringbeck and D. U. Sauer, Post-Mortem Analysis of Inhomogeneous Induced Pressure on Commercial Lithium-Ion Pouch Cells and Their Effects, *Sustainability*, 2019, **11**, 6738, DOI: 10.3390/su11236738.

11 T. Waldmann, B.-I. Hogg, M. Kasper, S. Grolleau, C. G. Couceiro, K. Trad, B. P. Matadi and M. Wohlfahrt-Mehrens, Interplay of Operational Parameters on Lithium Deposition in Lithium-Ion Cells: Systematic Measurements with Reconstructed 3-Electrode Pouch Full Cells, *J. Electrochem. Soc.*, 2016, **163**, A1232–A1238, DOI: 10.1149/2.0591607jes.

12 F. Ringbeck, C. Rahe, G. Fuchs and D. U. Sauer, Identification of Lithium Plating in Lithium-Ion Batteries by Electrical and Optical Methods, *J. Electrochem. Soc.*, 2020, **167**, 090536, DOI: 10.1149/1945-7111/ab8f5a.

13 T. Waldmann, B.-I. Hogg and M. Wohlfahrt-Mehrens, Li plating as unwanted side reaction in commercial Li-ion cells – a review, *J. Power Sources*, 2018, **384**, 107–124, DOI: 10.1016/j.jpowsour.2018.02.063.

14 P. P. Paul, E. J. McShane, A. M. Colclasure, N. Balsara, D. E. Brown, C. Cao, B.-R. Chen, P. R. Chinnam, Y. Cui, E. J. Dufek, D. P. Finegan, S. Gillard, W. Huang, Z. M. Konz, R. Kostecki, F. Liu, S. Lubner, R. Prasher, M. B. Preefer, J. Qian, M.-T. F. Rodrigues, M. Schnabel, S.-B. Son, V. Srinivasan, H.-G. Steinrück, T. R. Tanim, M. F. Toney, W. Tong, F. Usseglio-Viretta, J. Wan, M. Yusuf, B. D. McCloskey and J. Nelson Weker, A Review of Existing and Emerging Methods for Lithium Detection and Characterization in Li-Ion and Li-Metal Batteries, *Adv. Energy Mater.*, 2021, **11**, 2100372, DOI: 10.1002/aenm.202100372.

15 S. M. Abbas, C. Drießen, M. Sprenger, C. Ellersdorfer, I. Hanzu and G. Gstrein, Nondestructive Electrochemical Identification of Lithium Plating in High-Energy Automotive Batteries, *ACS Omega*, 2025, **10**, 13209–13217, DOI: 10.1021/acsomega.4c10805.

16 X. Lin, K. Khosravinia, X. Hu, J. Li and W. Lu, Lithium Plating Mechanism, Detection, and Mitigation in Lithium-Ion Batteries, *Prog. Energy Combust. Sci.*, 2021, **87**, 100953, DOI: 10.1016/j.pecs.2021.100953.

17 M. Sprenger, N. Dölle, F. Schauwecker, M. Raffler, C. Ellersdorfer and W. Sinz, Multiscale Analysis and Safety Assessment of Fresh and Electrical Aged Lithium-Ion Pouch Cells Focusing on Mechanical Behavior, *Energies*, 2022, **15**, 847, DOI: 10.3390/en15030847.

18 G. Zhang, X. Wei, G. Han, H. Dai, J. Zhu, X. Wang, X. Tang and J. Ye, Lithium plating on the anode for lithium-ion batteries during long-term low temperature cycling, *J. Power Sources*, 2021, **484**, 229312, DOI: 10.1016/j.jpowsour.2020.229312.

19 T. Waldmann, A. Iturrondobeitia, M. Kasper, N. Ghanbari, F. Aguesse, E. Bekaert, L. Daniel, S. Genies, I. J. Gordon, M. W. Löble, E. de Vito and M. Wohlfahrt-Mehrens, Review—Post-Mortem Analysis of Aged Lithium-Ion Batteries: Disassembly Methodology and Physico-Chemical

Analysis Techniques, *J. Electrochem. Soc.*, 2016, **163**, A2149–A2164, DOI: **10.1149/2.1211609jes**.

20 U. Janakiraman, T. R. Garrick and M. E. Fortier, Review—Lithium Plating Detection Methods in Li-Ion Batteries, *J. Electrochem. Soc.*, 2020, **167**, 160552, DOI: **10.1149/1945-7111/abd3b8**.

21 Y. Kobayashi, T. Kobayashi, K. Shono, Y. Ohno, Y. Mita and H. Miyashiro, Decrease in Capacity in Mn-Based/Graphite Commercial Lithium-Ion Batteries, *J. Electrochem. Soc.*, 2013, **160**, A1181–A1186, DOI: **10.1149/2.071308jes**.

22 T. C. Bach, S. F. Schuster, E. Fleder, J. Müller, M. J. Brand, H. Lorrmann, A. Jossen and G. Sextl, Nonlinear aging of cylindrical lithium-ion cells linked to heterogeneous compression, *J. Energy Storage*, 2016, **5**, 212–223, DOI: **10.1016/j.est.2016.01.003**.

23 M. Ecker, P. Shafiei Sabet and D. U. Sauer, Influence of operational condition on lithium plating for commercial lithium-ion batteries – Electrochemical experiments and post-mortem-analysis, *Appl. Energy*, 2017, **206**, 934–946, DOI: **10.1016/j.apenergy.2017.08.034**.

24 A. B. Gunnarsdóttir, C. V. Amanchukwu, S. Menkin and C. P. Grey, Noninvasive *In Situ* NMR Study of "Dead Lithium" Formation and Lithium Corrosion in Full-Cell Lithium Metal Batteries, *J. Am. Chem. Soc.*, 2020, DOI: **10.1021/jacs.0c10258**.

25 R. Bhattacharyya, B. Key, H. Chen, A. S. Best, A. F. Hollenkamp and C. P. Grey, In situ NMR observation of the formation of metallic lithium microstructures in lithium batteries, *Nat. Mater.*, 2010, **9**, 504–510, DOI: **10.1038/nmat2764**.

26 H. J. Chang, N. M. Trease, A. J. Ilott, D. Zeng, L.-S. Du, A. Jerschow and C. P. Grey, Investigating Li Microstructure Formation on Li Anodes for Lithium Batteries by *In Situ* 6 Li/7 Li NMR and SEM, *J. Phys. Chem. C*, 2015, **119**, 16443–16451, DOI: **10.1021/acs.jpcc.5b03396**.

27 K. Märker, C. Xu and C. P. Grey, Operando NMR of NMC811/Graphite Lithium-Ion Batteries: Structure, Dynamics, and Lithium Metal Deposition, *J. Am. Chem. Soc.*, 2020, DOI: **10.1021/jacs.0c06727**.

28 L. Sannier, R. Bouchet, S. Grugeon, E. Naudin, E. Vidal and J.-M. Tarascon, Room temperature lithium metal batteries based on a new Gel Polymer Electrolyte membrane, *J. Power Sources*, 2005, **144**, 231–237, DOI: **10.1016/j.jpowsour.2004.11.064**.

29 F. Orsini, A. Du Pasquier, B. Beaudoin, J. Tarascon, M. Trentin, N. Langenhuizen, E. de Beer and P. Notten, *In situ* Scanning Electron Microscopy (SEM) observation of interfaces within plastic lithium batteries, *J. Power Sources*, 1998, **76**, 19–29, DOI: **10.1016/S0378-7753(98)00128-1**.

30 W. Mei, L. Jiang, C. Liang, J. Sun and Q. Wang, Understanding of Li-plating on graphite electrode: detection, quantification and mechanism revelation, *Energy Storage Mater.*, 2021, **41**, 209–221, DOI: **10.1016/j.ensm.2021.06.013**.

31 F. Sagane, R. Shimokawa, H. Sano, H. Sakaebe and Y. Iriyama, In-situ scanning electron microscopy observations of Li plating and stripping reactions at the lithium phosphorus oxynitride glass electrolyte/Cu interface, *J. Power Sources*, 2013, **225**, 245–250, DOI: **10.1016/j.jpowsour.2012.10.026**.

32 H. You, B. Jiang, J. Zhu, X. Wang, G. Shi, G. Han, X. Wei and H. Dai, In-situ quantitative detection of irreversible lithium plating within full-lifespan of lithium-ion batteries, *J. Power Sources*, 2023, **564**, 232892, DOI: **10.1016/j.jpowsour.2023.232892**.

33 K. Sun, X. Li, Z. Zhang, X. Xiao, L. Gong and P. Tan, Pattern Investigation and Quantitative Analysis of Lithium Plating under Subzero Operation of Lithium-Ion Batteries, *ACS Appl. Mater. Interfaces*, 2023, **15**(30), 36356–36365, DOI: **10.1021/acsami.3c07098**.

34 T. Waldmann, M. Wilka, M. Kasper, M. Fleischhammer and M. Wohlfahrt-Mehrens, Temperature dependent ageing mechanisms in Lithium-ion batteries – A Post-Mortem study, *J. Power Sources*, 2014, **262**, 129–135, DOI: **10.1016/j.jpowsour.2014.03.112**.

35 Y. Liu, Y. Xia and Q. Zhou, Effect of low-temperature aging on the safety performance of lithium-ion pouch cells under mechanical abuse condition: a comprehensive experimental investigation, *Energy Storage Mater.*, 2021, **40**, 268–281, DOI: **10.1016/j.ensm.2021.05.022**.

36 D. Luo, M. Li, Y. Zheng, Q. Ma, R. Gao, Z. Zhang, H. Dou, G. Wen, L. Shui, A. Yu, X. Wang and Z. Chen, Electrolyte Design for Lithium Metal Anode-Based Batteries Toward Extreme Temperature Application, *Adv. Sci.*, 2021, **8**(18), 2101051, DOI: **10.1002/advs.202101051**.

37 M. M. Markowitz and D. A. Boryta, Lithium Metal–Gas Reactions, *J. Chem. Eng. Data*, 1962, **7**(4), 586–591, DOI: **10.1021/je60015a047**.

38 J. Cannarella and C. B. Arnold, The Effects of Defects on Localized Plating in Lithium-Ion Batteries, *J. Electrochem. Soc.*, 2015, **162**, A1365, DOI: **10.1149/2.1051507jes**.

39 M. Uitz, M. Sternad, S. Breuer, C. Täubert, T. Traußnig, V. Hennige, I. Hanzu and M. Wilkening, Aging of Tesla's 18650 Lithium-Ion Cells: Correlating Solid-Electrolyte-Interphase Evolution with Fading in Capacity and Power, *J. Electrochem. Soc.*, 2017, **164**, A3503, DOI: **10.1149/2.0171714jes**.

40 M. A. Hope, B. L. D. Rinkel, A. B. Gunnarsdóttir, K. Märker, S. Menkin, S. Paul, I. V. Sergeyev and C. P. Grey, Selective NMR observation of the SEI-metal interface by dynamic nuclear polarisation from lithium metal, *Nat. Commun.*, 2020, **11**, 2224, DOI: **10.1038/s41467-020-16114-x**.

41 Y.-C. Hsieh, M. Leißing, S. Nowak, B.-J. Hwang, M. Winter and G. Brunklaus, Quantification of Dead Lithium *via In Situ* Nuclear Magnetic Resonance Spectroscopy, *Cell Rep. Phys. Sci.*, 2020, **1**(8), 100139, DOI: **10.1016/j.xcrp.2020.100139**.

42 H. Zhou, C. Fear, R. E. Carter, C. T. Love and P. P. Mukherjee, Correlating lithium plating quantification with thermal safety characteristics of lithium-ion batteries, *Energy Storage Mater.*, 2024, **66**, 103214, DOI: **10.1016/j.ensm.2024.103214**.

43 Y. Wang, D. Dang, M. Wang, X. Xiao and Y.-T. Cheng, Mechanical behavior of electroplated mossy lithium at

room temperature studied by flat punch indentation, *Appl. Phys. Lett.*, 2019, **115**, 043903, DOI: 10.1063/1.5111150.

44 Y. Chen, L. Torres-Castro, K.-H. Chen, D. Penley, J. Lamb, M. Karulkar and N. P. Dasgupta, Operando detection of Li plating during fast charging of Li-ion batteries using incremental capacity analysis, *J. Power Sources*, 2022, **539**, 231601, DOI: 10.1016/j.jpowsour.2022.231601.